



HAL
open science

Disturbance and recovery in high speed (110) cleavage in single crystalline silicon

Lv Zhao, Meng Wang, Anne Maynadier, Daniel Nelias

► **To cite this version:**

Lv Zhao, Meng Wang, Anne Maynadier, Daniel Nelias. Disturbance and recovery in high speed (110) cleavage in single crystalline silicon. *Journal of the European Ceramic Society*, 2018, 38 (4), pp.1038 - 1045. 10.1016/j.jeurceramsoc.2017.12.035 . hal-02130058

HAL Id: hal-02130058

<https://hal.science/hal-02130058>

Submitted on 15 May 2019

HAL is a multi-disciplinary open access archive for the deposit and dissemination of scientific research documents, whether they are published or not. The documents may come from teaching and research institutions in France or abroad, or from public or private research centers.

L'archive ouverte pluridisciplinaire **HAL**, est destinée au dépôt et à la diffusion de documents scientifiques de niveau recherche, publiés ou non, émanant des établissements d'enseignement et de recherche français ou étrangers, des laboratoires publics ou privés.

1 **Disturbance and recovery in high speed (110) cleavage in**
2 **single crystalline silicon**

3 **Lv Zhao · Meng Wang · Anne Maynadier ·**
4 **Daniel Nelias**

5
6 Received: date / Accepted: date

7 **Abstract** Stress perturbations and material defects can significantly affect the
8 fracture initiation and propagation behaviors in brittle materials. In this work, we
9 show that (110) [110] cleavage in silicon deflects onto (111) plane in the presence
10 of contact stresses. The deflection is however not permanent as the crack returns
11 to the (110) plane after a certain length of propagation, even in the case where
12 the crack velocity is up to 78% of the Rayleigh wave speed. The recovery behavior
13 indicates that the (110) [110] cleavage is invariably prevailing when perpendicular
14 to the maximum stress. Following this indication, it can be concluded that the
15 observed (110) [110]–(111) deflection in previous literature is most likely driven by
16 the external disturbance rather than the crack velocity induced toughness evolu-
17 tion. We also highlight that the extra energy for the (110) recovery is minimized
18 at the expense of a large propagation distance upon the plane switch.

19 **Keywords** Fracture, silicon single crystal, crack deflection, high speed propaga-
20 tion

21 **1 Introduction**

22 Crystalline silicon occupies a dominant place in the current photovoltaic (PV)
23 applications. However, due to the brittle characteristic, catastrophic failure of the
24 solar cells eventually leads to large power loss and severely impacts reliability and

Lv Zhao
Univ Lyon, INSA-Lyon, CNRS UMR5259, LaMCoS, F-69621, France
E-mail: lv.zhao08@gmail.com

Meng Wang
Univ Lyon, INSA-Lyon, CNRS UMR5259, LaMCoS, F-69621, France

Anne Maynadier
Univ Bourgogne Franche Comté, FEMTO-ST Institute, Departement of Applied Mechanics,
CNRS/UFC/ENSMM/UTBM, F-25000, France

Daniel Nelias
Univ Lyon, INSA-Lyon, CNRS UMR5259, LaMCoS, F-69621, France
E-mail: daniel.nelias@insa-lyon.fr

durability of the Si-based PV technology [1,2]. A full understanding on the fracture mechanism in silicon is necessary for the design and the use of PV devices. Albeit continuous investigations have been performed, the fracture behaviors, particularly those manifest during the dynamic propagation, still involve an open discussion [3,4].

The fracture in silicon mainly takes place along the low energy planes of (110) and (111) [5–8]. The crack velocity in silicon is generally high because of the low fracture toughness and the absence of plastic dissipation under the brittle-ductile transition temperature [9–11]. Among the velocity related fracture phenomena, velocity gap received a significant attention. Experiments showed that low ($\ll 2000$ m/s) steady state crack velocity was somehow forbidden [6,12], conversely to the theoretical one that can vary from zero to the Rayleigh wave speed (C_R) according to the linear fracture mechanics. Molecular dynamics simulations explained this threshold as a consequence of a localized phase transformation in the vicinity of the crack tip [13] that delays the fracture initiation. However, a recent work suggested that the velocity gap should not be considered as an universal indication, since an extremely low speed (in 100 m/s speed range) cleavage along (110) can stably take place via kink formation and advance under a suitable temperature and some specific loading conditions [14]. This new finding reveals that the external conditions need to be carefully considered when investigating the fracture in silicon.

As one of the main crack paths in single crystalline silicon, (110) cleavage has been substantially investigated in the previous literature [12,15,16]. Pioneer works highlighted that (110) cleavage involved a directional anisotropy [8,15]. The crack propagation in [001] direction on the (110) plane (denoted as (110) [001]) could not be achieved and the crack systematically switched to (111) plane [7]. This deflection mechanism was elucidated by molecular dynamics simulations [8,15], which showed that the atom debonding suffered from pronounced lattice trapping when heading (110) [001].

Conversely to the (110) [001] cleavage that would yield a global plane deflection, (110) [110] crack manifests with a much higher stability [12]. Mirror-like morphology was observed in the middle of the (110) fracture surface during a high speed propagation (3000 m/s) under tension, accompanied by tiny (111) facets near the specimen surface [12]. This stability was also evidenced in 4-line bending tests (with the crack propagates in the middle of the contact span), in which the (110) plane was dominant up to the propagation velocity of 3700 m/s [16]. However, 3-line bending conditions (with the crack propagates underneath the punch roller) led to disparate fracture scenarios [17,18]. In these experiments, large (110)–(111) plane deflection was encountered when the crack velocity exceeded 2000 m/s. Regarding the explanation for the deflection phenomenon, the authors conjectured that the (110) dynamic toughness would increase faster than that of the (111) plane when the crack speeds up, so that till a certain velocity (for instance 2900 m/s in the [110] direction) the (110) plane becomes no longer the prevailing crack path in a high speed case [17,19]. After that, a thermal phonon emission mechanism was postulated, which permitted to rationalize the aforementioned conjecture [20]. However, the plane switch theory derived from these 3-line bending tests might not be generalized, since i) the presence of the external perturbations, *i.e.* the contact stresses was not taken into account, and ii) (110) [110] cleavage was revealed stable regardless of the crack velocity (1200 m/s–3700 m/s)

when subjected to pure bending load [16]. From these two attributes, it brings the need for a revision of (110) [110] cleavage, and the fracture stability should be assessed with the careful measures of external perturbations during high speed crack propagations.

Therefore, in the present work, we investigate the (110) [110] initiation and propagation behaviors in the presence of the contact conditions and also with various micro-crack geometries. 4-line bending tests are performed using single crystalline silicon wafer without pre-existing cracks. The absence of pre-cracks not only favors the initiation under the punch roller, but also promotes large crack velocity. High speed camera is used to monitor the first crack, then fractographic analysis is carried out to identify the cleavage plane and to determine the crack velocity during the propagation. It is observed that the crack tends to switch to the (111) plane at the early propagation stage. However, the disturbance is not permanent as the crack systematically recovers on the (110) plane after a certain length of propagation. Moreover, the recovery occurs over an extremely high velocity (3500 m/s *i.e.* $0.78C_R$). This indicates that the (110) [110] crack path is more energetically favorable than the (111) ¹ one in both slow and rapid propagations, which is contradictory to the aforementioned evolution mechanism of the fracture toughness.

2 Experiments

2.1 Single crystalline silicon plate

Solar grade single crystalline silicon was used. The specimens were cut from as-sawn silicon wafers. The dimension of the specimens is $50 \times 50 \times 0.2$ mm. The crystal is oriented such that two [110] directions are parallel with the specimen edges and one [100] direction perpendicular to the specimen surface.

As shown in Fig. 1, the specimen surface involves periodic cutting traces and also some hollows (see Fig. 1(a)). The hollows can be more clearly evidenced in Fig. 1(b). This surface morphology is attributed to the diamond wire sawing process where the hard diamond particles indent the new created silicon surface and lead to lateral cracks (manifesting as hollows in Fig. 1(b)). The interaction is shown in the schematic Fig. 1(c). Along with the lateral cracks, sharp median cracks likely nucleate and extend into the material. This kind of cracks, which are barely visible under microscope, have been monitored by X-ray image and shown to have a depth of 10 μm range [21]. These micro-cracks are randomly distributed on the specimen surface.

2.2 4-line bending tests

A 4-line bending set up was used to load the samples til fracture. The silicon plate was placed such that the (110) [110] was right aligned with the punch roller, see Fig. 2. In this configuration, the (110) plane would be the most solicited as it is perpendicular to the maximum stress. The inner and outer contact spans

¹ In a loading configuration where the maximum stress is perpendicular to the (110) plane.

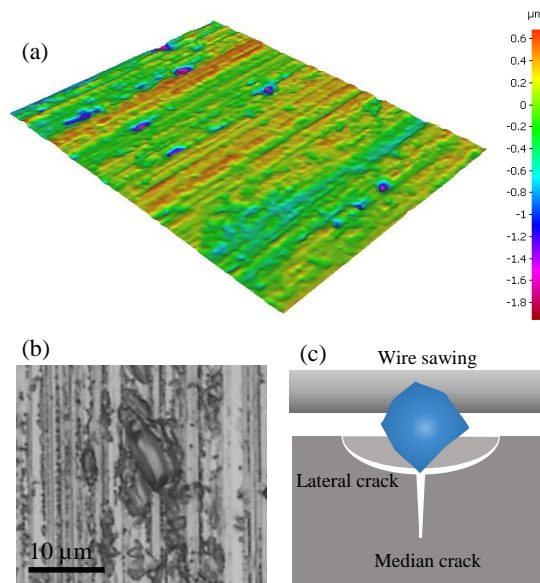


Fig. 1: Morphology of the specimen surface. Distribution of cutting traces and hollows (a), zoom on one hollow (b), schematic drawing of lateral and median cracks induced by diamond particle-material interaction (c).

114 are 21 mm and 40 mm, respectively. Quasi-static loading conditions with a strain
 115 rate in the order of $10^{-6}/s$ were ensured by a LLOYD-Ametek LFPLUS electro-
 116 mechanical machine.

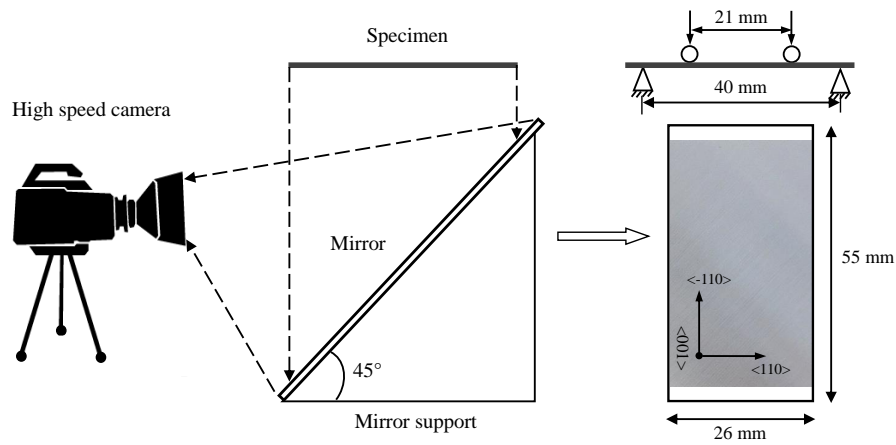


Fig. 2: 4-line bending instrumented with a high speed camera.

117 2.3 Fracture monitoring

118 A high speed camera (Phantom V710) was set up in order to capture the fracture
119 initiation and propagation. Given that the initiation would most likely occur under
120 the punch roller, the camera was set as it could cover the whole inner contact
121 region, see Fig. 2. As a compromise, the frequency for image acquisition was set
122 to 49000 Hz at the expense of the image resolution (512×256 pixels).

123 Fractographic analysis was carried out after each test to evaluate in a post-
124 mortem way the cleavage plane as well as the crack velocity. The crack velocity
125 estimation was based on our former work [16], in which a correlation between the
126 crack surface morphology and the propagation velocity was established. In this
127 way, the resolution for velocity measurement was down to micro-scale along the
128 propagation path and the steady state of the crack propagation could be easily
129 identified.

130 3 Results

131 The results will be presented in two parts, in each a representative case is ad-
132 dressed. The first one shows the contact perturbations, the second one exhibits
133 the effect induced by the orientation of the fracture origin. For each part, the frac-
134 ture initiation is highlighted with the high speed imaging technique and the local
135 crack propagation is disclosed with the fractographic analysis. A general discussion
136 on the fracture behavior will finally be carried out in the next section.

137 3.1 Contact perturbations

138 The fracture process of the first case is presented in Fig. 3a. The image #0 rep-
139 resents the last photo before cracking. The image #1 monitors the first crack, it
140 involves a subtraction between the first photo after cracking and #0. The image
141 #2, which is the second photo after cracking, shows multiple cracks right after
142 the fracture initiation. From #1, it can be noticed that the first crack nucleates
143 and propagates straightly right underneath the punch roller. The image #2 re-
144 veals that secondary cracks are curved and involve some branching instabilities.
145 This multiple cracking feature is attributed to a burst of flexural waves that are
146 generated upon the sudden release of the curvature of the bent specimen [22]. The
147 flexural waves then lead to local overstresses and initiate secondary cracks.

148 According to the observations on the first crack, the fracture initiation spot
149 and the cleavage planes during the propagation are reconstructed and presented
150 in Fig. 3b. One can notice that the crack initiates from a sub-surface micro-crack
151 which should be induced by the wire sawing. The fracture origin is located near the
152 half length of the specimen, so the crack propagates in two opponent directions.
153 The fracture history for this case is outlined below:

- 154 – The fracture initiation takes place on the (110) plane. Very smooth fracture
155 surface can be noticed close to the initiation spot, as shown in the schematic
156 drawing in Fig. 3b. This indicates that the micro-crack is oriented nearly par-
157 allel to the (110) plane, which ensures a small mismatch between the fracture
158 origin and the very beginning cleavage path.

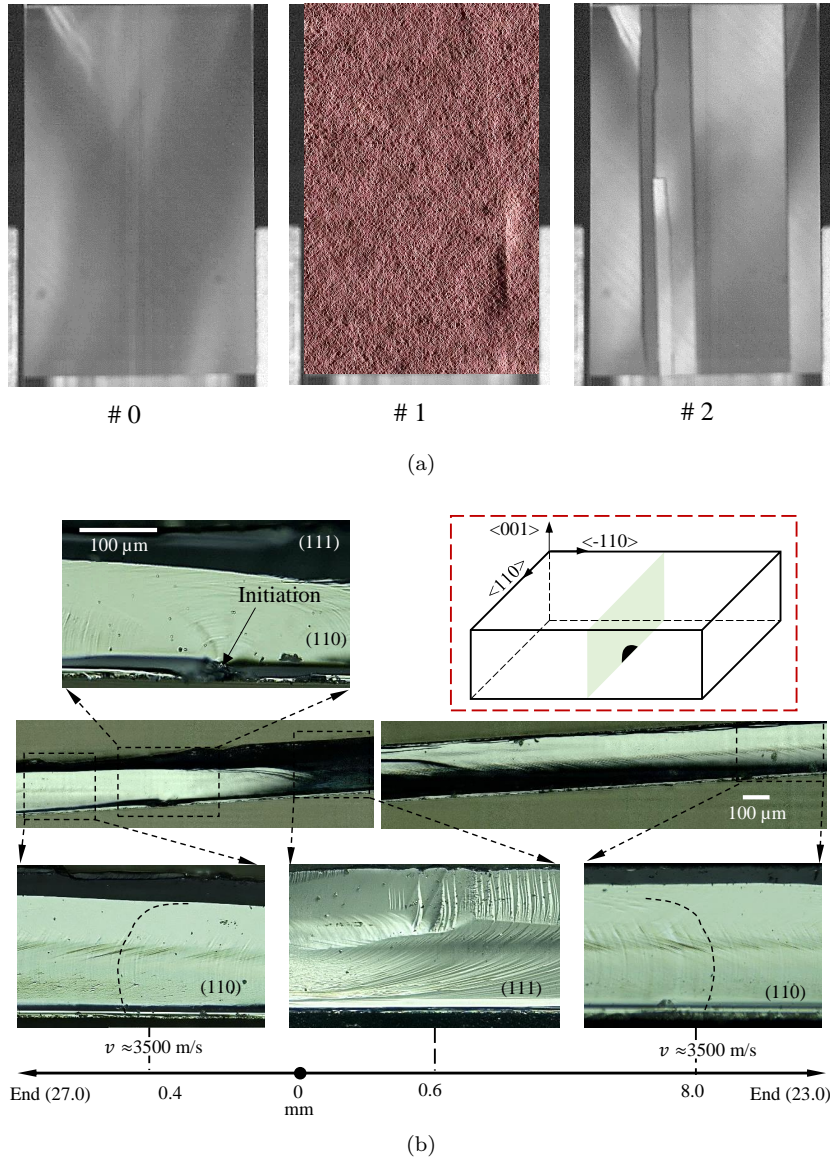


Fig. 3: Crack deflection and recovery under contact perturbations. First crack monitoring (a), and fractographic reconstruction of the crack initiation and propagation (b). The dotted curved lines in (b) represent the Wallner lines.

- 159 – The crack switches to a (111) plane after a very short propagation to the right
 160 side, while it remains on the (110) plane during the subsequent propagation.
 161 The deflection part manifests as a black zone on the fractography, as can be
 162 noticed in the long fractographic images in Fig. 3b.

- 163 – After a propagation of about 8 mm to the right side on the (111) plane, the
 164 crack returns to the initial (110) plane and then propagates in a steady state.
 165 The steady state is clearly indicated by the constant shape of the Wallner
 166 lines [16], see Fig. 3b.
- 167 – From the morphology of the fracture surface, one can infer that the steady
 168 state crack velocities are close for both sides, which are equal to about 3500
 169 m/s. This velocity represents 78% of the Rayleigh wave speed.

170 The global fracture path for the present case is illustrated in Fig. 4 to show
 171 the deflection behaviors. The deflection first nucleates when the crack extends to
 172 the compression side of the specimen, this is also where the contact would have
 173 strong perturbations in the stress field. This deflection then quickly develops to the
 174 tensile side until the (111) plane covers the whole fracture surface. Therefore, it
 175 can be concluded that the contact significantly influences the (110) [110] cleavage
 176 and ultimately leads to a global plane deflection. This conclusion can explain why
 177 (111) cleavage was encountered in 3-line bending tests [17].

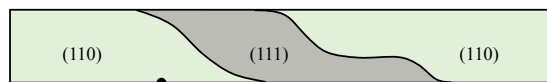


Fig. 4: Overall fracture path under the contact perturbations.

178 However, the (110) [110]-(111) deflection is not permanent. According to the
 179 observations in the present work, the crack recovers the (110) plane after a certain
 180 length of propagation. This recovery was not observed in the previous 3-line bend-
 181 ing tests. Interestingly, with other 3 similar tests, it is found that the recovery is
 182 repeatable and always takes place at a distance around 8 mm from the initiation
 183 point.

184 3.2 Fracture origin orientation

185 The present section addresses the second case in which the effect of the fracture
 186 origin orientation is involved. The identification of the first crack is presented
 187 in Fig. 5a. The numberings #0, #1 and #2 have the same representations as
 188 explained in section 3.1. Here, in the image #1, several cracks can be noticed.
 189 Among them, the left one, which is right underneath the punch roller, is the
 190 longest and therefore considered as the first crack.

191 Focusing on the first crack, the fracture initiation and propagation are disclosed
 192 by fractography, as can be noticed in Fig. 5b. The fracture origin involves also the
 193 sub-surface micro-crack, which is located 17 mm away from one of the specimen
 194 edges. Following observations are exhibited which allow an overview on the fracture
 195 process:

- 196 – The crack initiates on the (111) plane. This crack nucleation is due to the fact
 197 that the micro-crack orientation is closer to the (111) plane, as indicated in
 198 the schematic drawing in Fig. 5b. Yet the contact stresses are not relevant,
 199 knowing that the fracture origin is on the tensile side of the specimen and

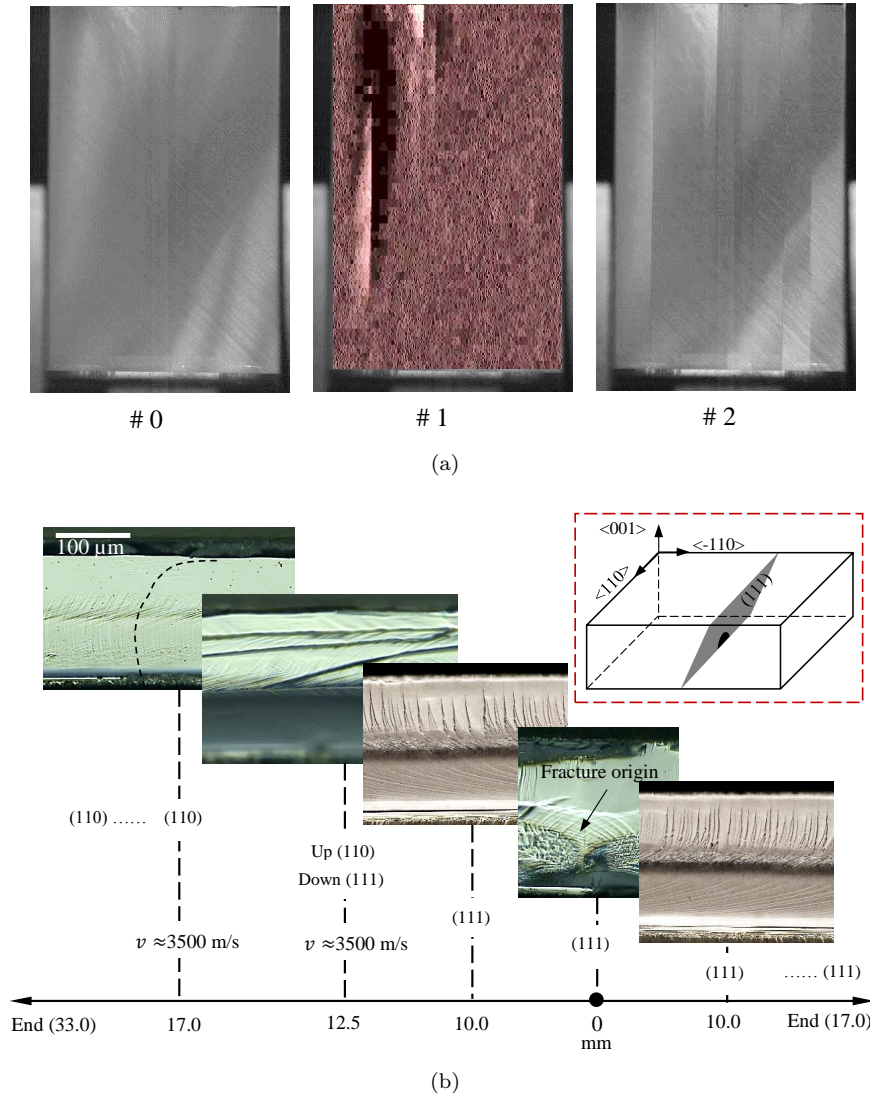


Fig. 5: Crack deflection and recovery under contact perturbations as well as (111) oriented fracture origin. First crack monitoring (a), and fractographic reconstruction of the crack initiation and propagation (b). The dotted curved lines in (b) represent the Wallner lines.

200 thus far from the contact perturbations. The crack initiation involves the main
 201 difference between the present case and the one presented in section 3.1.
 202 – The crack propagates along the (111) plane to the right side at a quite constant
 203 velocity, *i.e.* in its steady state, till reaching one free edge of the specimen. The
 204 steady state is revealed by the morphology of the (111) instabilities [23,24], as

- 205 shown in the right image in Fig. 5b. The length of the trajectory is about 17
 206 mm.
- 207 – To the left side, the crack initially continues with a steady state (111) cleavage.
 208 Then, it begins to progressively deflect onto the (110) plane after a propagation
 209 length of 12 mm. The deflection is finished at about 17 mm away from the
 210 initiation point. The crack then propagates stably on the (110) plane until it
 211 reaches the other specimen edge.
 - 212 – Thanks to the Wallner line shape, the velocity is estimated around 3500 m/s
 213 for the (110) part, which reaches nearly 78% of the Rayleigh wave speed. The
 214 velocity cannot be inferred on the (111) plane, as the Wallner lines are not
 215 noticeable because of the surface instabilities.

216 The whole crack path for the present case is schematized in Fig. 6. Since both
 217 the contact perturbations and the fracture origin-(110) plane mismatch are present
 218 in this case, the (111) part is much longer (17 mm) than that in the case where
 219 only the contact perturbations are involved (8 mm), see Fig. 3b. It should be noted
 220 that the difference is not related to the crack velocity, as the steady state velocities
 221 are very close in both cases.

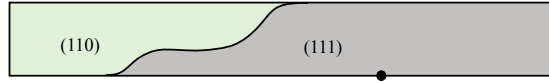


Fig. 6: Overall fracture path under the contact perturbations as well as (111) oriented fracture origin.

222 Despite of the strong perturbations, the crack jumps to the (110) plane after
 223 a long propagation. It should be noted that the deflection process in Fig. 6 is
 224 almost the same as that presented in Fig. 4. It begins from the upper portion of
 225 the fracture surface and then develops towards the lower portion until the (110)
 226 plane covers the whole fracture surface. This deflection behavior will be discussed
 227 in the following section.

228 4 Discussion

229 Albeit the (111) plane has the smallest fracture toughness ($\Gamma_{(111)}=2.88 \text{ J/m}^2$),
 230 in the present loading configuration (see Fig. 2), the fracture energy dissipation
 231 ($\Gamma_{(111)}^*=3.54 \text{ J/m}^2$) is however larger compared to the (110) plane ($\Gamma_{(110)}^*=3.46$
 232 J/m^2) because of the 35.6° inclination (see Figs. 3b and 5b). Thus, the (110)
 233 plane is dominant in low speed fracture ($\approx 1000 \text{ m/s}$), as highlighted in previous
 234 works [16–18]. Nonetheless, it still remains unclear on the fracture mechanism in
 235 the high speed cases, considering different fracture paths reported when the crack
 236 velocity exceeds 2000 m/s [16, 17]. In this work, it has been shown that the crack
 237 either stably propagates along the (110) [110] path or switches from the (111) plane
 238 to this path at very high velocities ($>3000 \text{ m/s}$). It can thus be concluded that the
 239 (110) [110] cleavage remains energetically prevailing compared to the (111) one in
 240 very high speed cases. In the one hand, this conclusion is coherent with our former

241 work [16] in which it was found that in the absence of perturbations the crack
 242 always chooses the (110) plane for a large range of crack velocities [1200 m/s–3700
 243 m/s]. In the other hand, the dynamic toughness evolution proposed in the previous
 244 literature [17, 19] cannot be generalized since it cannot be substantiated by the
 245 fracture behavior revealed in our former work [16] as well as the present one.

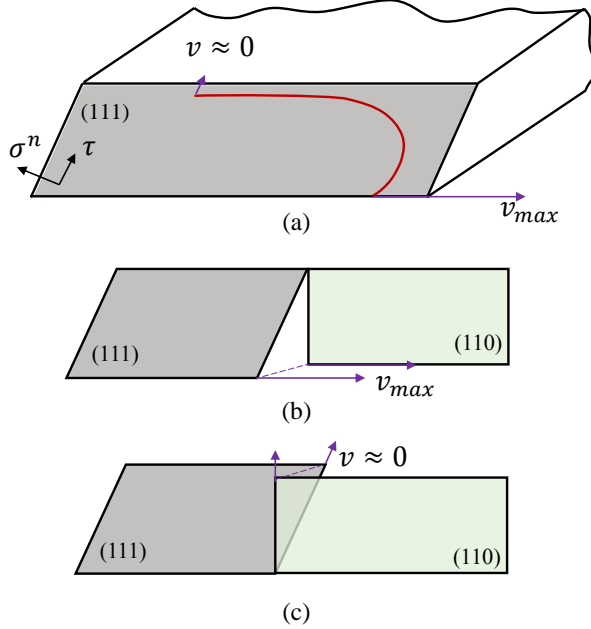


Fig. 7: (111)-(110) deflection. The crack propagates on the (111) plane under bending (a), possibility of deflection from the lower portion (b), and possibility of deflection from the upper portion (c).

246 As revealed through the experimental results, the contact effect and the (111)
 247 oriented defect drive the crack to deflect or initiate on the (111) plane. Then a
 248 recovery to the (110) plane takes place as the crack propagates far away from
 249 the perturbation origin. However, the (111)–(110) deflection needs extra energy.
 250 This can be assimilated to a grain boundary crossing. Previous studies have
 251 shown that when a crack switches from one grain to the adjacent one, the mis-
 252 orientation between the two cleavage planes toughens the plane ahead the grain
 253 boundary [25]. In this sense, if the deflection is instant or very short, the (110)
 254 plane will become no longer favorable since it is toughened due to a rotation of
 255 35.6° ($\Gamma_{(110)}^{**} = \Gamma_{(110)}^* / \cos(35.6^\circ) = 4.25 \text{ J/m}^2$ compared to $\Gamma_{(111)}^* = 3.54 \text{ J/m}^2$). There-
 256 fore, in order to avoid the strong toughening induced by the sudden plane change,
 257 the (111)-(110) deflection involves a long process. As indicated in Fig. 4 and Fig. 6,
 258 the deflection takes place first in the upper portion of the fracture surface, where
 259 the crack velocity is very low, and then extends to the lower portion, where the
 260 crack velocity is much higher, until the (110) dominates the whole crack path. The
 261 extension covers a propagation length of about 5 mm for both cases presented in

262 section 3.1 and 3.2. This indicates that the (111)-(110) deflection is likely inde-
 263 pendent of the previous propagation history.

264 Why the (111)-(110) deflection initiates from the low speed portion? Indeed,
 265 when the crack switches from the (111) plane to the (110) one under bending, there
 266 exist two possibilities, as illustrated in Fig. 7. One is that the deflection initiates
 267 from the lowest point, where the local velocity coincides with the global velocity
 268 and is the largest, see Fig. 7(b), the other is from the highest point, where the local
 269 velocity is almost zero, see Fig. 7(c). Assuming that the deflection is instataneous,
 270 for the first possibility, the crack needs to rotate twice 90° , while a single rotation
 271 of 35.6° is involved for the second one. This clearly shows that the deflection will be
 272 much easier to take place from the upper portion in terms of avoding large angle
 273 mismatch during the deflection. Moreover, when the deflection begins from the
 274 highest point along the crack front, the deflection is naturally progressive as the
 275 lower part advances faster and will not be immediately affected by the deflection
 276 induced stress rearrangement. The deflection process is shown in the schematic
 277 illustration Fig. 8, which permits a full analysis on the local deflection behavior.
 278 Taking θ as the angle between the local crack velocity direction and the horizontal
 279 direction on the (111) plane, the local velocity direction along the crack front, as
 280 indicated by the dotted arrows in Fig.8, can be expressed as:

$$\mathbf{V} = [\cos(\theta), \sin(\theta), 0] \quad (1)$$

281 When the deflection towards the (110) plane happens at any point of the crack
 282 front, the local velocity direction, as indicated by the solid arrows in Fig.8 becomes:

$$\mathbf{V}' = [\cos(\theta), \sin(\theta)\cos(35.6^\circ), \sin(\theta)\sin(35.6^\circ)] \quad (2)$$

283 Therefore, the local deflection angle can be expressed in the function of θ ,
 284 which is also linked to the position along the crack front, as following:

$$\alpha = \arccos(\cos(\theta)^2 + \sin(\theta)^2 \cos(35.6^\circ)) \quad (3)$$

285 As the deflection extends to the lower portion *i.e.* θ varies from 90° to 0° , the
 286 deflection angle diminishes until zero at the lowest point, as can be noticed in
 287 Fig.9. At the same time, the local velocity v_l increases from zero to the maximum
 288 value v_{max} which is also the global crack velocity, as drawn in Fig.9. The local
 289 velocity is calculated according to the following approximation:

$$v_l = v_{max} \cos(\theta) \quad (4)$$

290 Thanks to to the Freund condition [26], the energy balance during the crack
 291 propagation is well established:

$$G_S = \frac{\Gamma_D C_R}{C_R - v} \quad (5)$$

292 where G_S denotes the static strain energy release rate, Γ_D represents the dy-
 293 namic toughness, C_R and v are the Rayleigh speed and the crack velocity, respec-
 294 tively.

295 It can be noted that higher the crack velocity is, larger the energy dissipation.
 296 The relationship can be noticed in Fig. 9. As the deflection angle decreases along
 297 with the local velocity increases, the deflection process that described in Fig.8

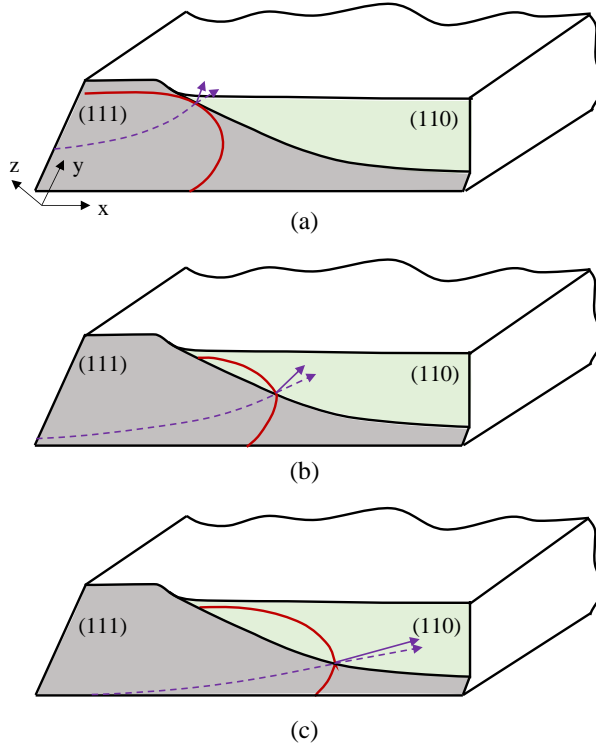


Fig. 8: Schematic process of the (111)-(110) deflection. The crack deflects from the upper portion (a), then it continues to deflect towards the lower portion (b) and (c). The dotted arrows indicate the atom debonding directions upon deflection and the solid arrows stand for the atom debonding directions if the crack remains on the (111) plane.

298 allows to minimize the extra energy dissipation to jump from the (111) plane to
 299 the (110) one. It should be noted that if the deflection starts from the lowest
 300 point, the overall dissipated extra energy for plane switch will be much higher,
 301 this in turn will strongly decrease the global crack velocity. In other words,
 302 the crack deflects from the highest point so that the global crack velocity would not
 303 be significantly affected.

304 To the best of the authors' knowledge, this is the first work showing both the
 305 (110)-(111) and the (111)-(110) deflections in the fracture process in silicon. The
 306 underlying mechanisms are however different for these two opponent plane switch
 307 scenarios. More importantly, the results in the present study raise an open discus-
 308 sion on the previous literature works in which dynamic toughness evolution was
 309 assessed [17]. Note also that this study is mainly focused on high speed cracking,
 310 which corresponds to large fracture stress and thus large contact force. In the fu-
 311 ture, the investigation can be completed by other experiments in which controlled
 312 fracture origin size can be ensured to have variant crack propagation velocities.

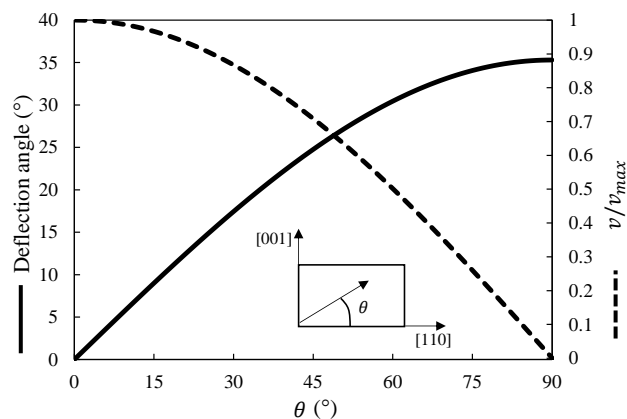


Fig. 9: Deflection angle and local crack velocity evolution along the crack front under bending. The deflection refers to the (111)–(110) cleavage plane switch.

313 5 Conclusion

314 In this work, the (110) [110] cleavage in silicon has been investigated in the presence
 315 of contact perturbations as well as including various fracture origin geometries. It
 316 has been shown that the contact can easily lead to (110)–(111) deflection, which
 317 however was previously considered as a consequence of high speed propagation.
 318 Albeit the external perturbations deviate the crack from the most favorable path,
 319 (111) plane cannot be permanently maintained and the fracture process involves a
 320 recovery to (110) [110] scenario during the propagation. This work highlights that
 321 the dynamic toughness of the (110) plane should not increase faster than that of
 322 the (111) plane until 78% of the Rayleigh wave speed. The (110) plane recovery
 323 initiates from the lowest velocity point and progressively extend to the highest
 324 velocity point in order to minimize the extra energy dissipation for the deflection.

325 Acknowledgment

326 The authors thank the French research agency ANR for partial funding through
 327 the DURASOL Equipex project.

328 References

- 329 1. M. Köntges, I. Kunze, S. Kajari-Schröder, X. Breitenmoser, B. Bjørneklett, Sol. Energy
 330 Materi. Sol. Cells **95**, 1131 (2011)
- 331 2. M. Paggi, I. Berardone, A. Infuso, M. Corrado, Sci. Rep. **4**, 4506 (2014)
- 332 3. M. Adda-Bedia, R.E. Arias, E. Bouchbinder, E. Katzav, Phys. Rev. Lett. **110**, 014302
 333 (2013)
- 334 4. E. Bitzek, J.R. Kermode, P. Gumbsch, Int. J. Fract. **191**, 13 (2015)
- 335 5. A. George, G. Michot, Mater. Sci. Eng. A **164**, 118 (1993)
- 336 6. D. Holland, M. Marder, Phys. Rev. Lett. **80**, 746 (1998)
- 337 7. F. Ebrahimi, L. Kalwani, Mater. Sci. Eng. A **268**, 116 (1999)
- 338 8. R. Pérez, P. Gumbsch, Acta Mater. **48**, 4517 (2000)
- 339 9. M. Brede, Acta Metall. Mater. **41**, 211 (1993)
- 340 10. J. Samuels, S.G. Roberts, Proc. R. Soc. London, Ser. A, Math. Phys. Sci. **421**, 1 (1989)
- 341 11. A. Masolin, P.O. Bouchard, R. Martini, M. Bernacki, J. Mater. Sci. **48**, 979 (2012)

-
- 342 12. T. Cramer, A. Wanner, P. Gumbsch, Phys. Rev. Lett. **85**, 788 (2000)
343 13. M.J. Buehler, H. Tang, A.C.T. van Duin, W.A. Goddard, Phys. Rev. Lett. **99**, 165502
344 (2007)
345 14. J.R. Kermode, A. Gleizer, G. Kovel, L. Pastewka, G. Csanyi, D. Sherman, A.D. Vita,
346 Phys. Rev. Lett. **115**, 135501 (2015)
347 15. R. Pérez, P. Gumbsch, Phys. Rev. Lett. **84**, 5347 (2000)
348 16. L. Zhao, D. Bardel, A. Maynadier, D. Nelias, Scr. Mater. **130**, 83 (2017)
349 17. D. Sherman, I. Be'ery, J. Mech. Phys. Solids **52**, 1743 (2004)
350 18. D. Sherman, I. Be'ery, Scr. Mater. **49**, 551 (2003)
351 19. D. Sherman, J. Mech. Phys. Solids **53**, 2742 (2005)
352 20. F. Atrash, D. Sherman, J. Mech. Phys. Solids **60**, 844 (2012)
353 21. H.J. Möller, C. Funke, M. Rinio, S. Scholz, Thin Solid Films **487**, 179 (2005)
354 22. B. Audoly, S. Neukirch, Phys. Rev. Lett. **95**, 095505 (2005)
355 23. D. Sherman, M. Markovitz, O. Barkai, J. Mech. Phys. Solids **56**, 376 (2008)
356 24. J. Kermode, L. Ben-Bashat, F. Atrash, J. Cilliers, D. Sherman, A.D. Vita, Nat. Commun.
357 **4**, 2441 (2013)
358 25. L. Zhao, D. Nelias, D. Bardel, A. Maynadier, P. Chaudet, B. Marie, J. Phys. D: Appl.
359 Phys. **49**(47), 475601 (2016)
360 26. L.B. Freund, *Dynamic fracture mechanics* (Cambridge University Press, 1990). Cambridge
361 Books Online